Journal of Translational Medicine

RESEARCH

Open Access

Formyl peptide receptor 2 activation by MR-39 inhibits glioblastoma cell proliferation and invasiveness through suppression of multiple oncogenic pathways

Maria Grazia Ferraro[1*†], Marco Bocchetti[2,3,4†], Marianna Affinito[5], Ercolano Giuseppe[5], Kardelen Dalim Filiz[5,9], Luisa Speranza[5], Enza Lacivita[6], Marcello Leopoldo[6], Marianna Crispino[7], Anna Ceccarelli[8], Carla Perrone-Capano[5], Maria Concetta Miniaci[5], Michele Caraglia[3,4] and Floriana Volpicelli[5*]

Abstract

Background Glioblastoma (GBM) is the most common, aggressive and poor prognosis malignant brain tumor in adults, that is still orphan of effective medical treatments. The formyl peptide receptor 2 (FPR2), a G protein– coupled receptor implicated in inflammation and cancer biology, has emerged as a potential therapeutic target, yet its role in GBM remains poorly defined.

Methods We investigated the effects of MR-39, a novel selective FPR2 agonist, in three human GBM cell lines (U87MG, U138-MG, U251-MG). Antiproliferative effects were assessed via CCK-8 assays, cell counts, Ki67 immunostaining, and cell cycle analysis. The specificity of MR-39 was tested using the FPR2 antagonist WRW4 and siRNA-mediated knockdown. Whole-transcriptome analysis, RT-qPCR, Western Blot, woundhealing assays, in vitro tube formation assay, and hypoxia models were used to explore its impact on invasion, angiogenesis, and hypoxia-driven pathways.

Results MR-39 significantly reduced proliferation in all GBM cell lines and induced a non-canonical, p53dependent S-phase arrest associated with the inhibition of both MAPK/ERK and AKT pathways. These effects were reversed by the FPR2 antagonist WRW4 or by FPR2 silencing. Transcriptomic and functional assays revealed downregulation of epithelial-to-mesenchymal transition (EMT) drivers, including Neuralcadherin (N-cadherin), Snail Family Transcriptional Repressor 2 (Slug), Snail Family Transcriptional Repressor 1 (Snail), matrix metalloproteinase-2 (MMP2), fibronectin 1 (FN1), and increased Epithelialcadherin (E-cadherin) expression, resulting in impaired migration. MR-39 displays anti-angiogenic and anti-hypoxia related activities, indeed it is able to inhibit Vascular Endothelial Growth Factor

[†]Maria Grazia Ferraro and Marco Bocchetti contributed equally to this work.

*Correspondence:
Maria Grazia Ferraro
mariagrazia.ferraro@unina.it
Floriana Volpicelli
floriana.volpicelli@unina.it

Full list of author information is available at the end of the article

(VEGF) and Vascular Endothelial-cadherin (VE-cadherin) expression, to disrupt endothelial network formation, and to attenuate Hypoxia Inducible Factor 1 Subunit Alpha (HIF-1α) stabilization under hypoxic conditions. Notably, MR-39 exhibited significant anti-inflammatory effects, as evidenced by the downregulation of pro-inflammatory genes, including Cyclooxygenase 2 (COX-2), Chemokine (C-X-C Motif) Ligand 7. (CXCL-7), Nuclear Factor Kappa B Subunit 1 (NFKB1), Interleukin 1 Beta (IL-1β), and Interleukin 6 (IL6), and the inhibition of NF-κB protein levels.

Conclusion This study identifies MR-39 as a potent modulator of FPR2, and identifies its mechanisms of action in GBM, such as anti-tumor activity, including S-phase arrest, inhibition of EMT, and suppression of both angiogenesis and hypoxic adaptation. By directing FPR2 signaling toward an anti-tumor profile, MR-39 represents a promising therapeutic candidate for GBM.

Keywords AKT pathway, Angiogenesis, Epithelial-to-Mesenchymal Transition (EMT), FPR2, Hypoxic adaptation, MAPK/ERK pathways, S-phase arrest

Background

Glioblastoma (GBM) is the most aggressive and prevalent primary malignant brain tumor in adults, accounting for 45–50% of all malignant brain tumors. Its global incidence is approximately 3.19 per 100,000 individuals, with the highest occurrence in patients over 65 years of age. The disease shows a slight male predominance and is more common among Caucasian individuals [1, 2]. Clinically, GBM is one of the most treatment-resistant cancers, characterized by rapid proliferation, extensive invasiveness, and pronounced heterogeneity [3]. The current standard of care for GBM involves maximal safe surgical resection, followed by combined radiotherapy and concurrent temozolomide chemotherapy. This offers only limited benefits, with a median survival remaining 15–18 months and a 5-year survival rate below 10% [1, 4]. Cancer recurrence occurs frequently, leading to treatment failure and ultimately death. These disappointing outcomes highlight the urgent need for novel therapeutic strategies and molecular targets.

Two adaptive programs are mainly responsible for GBM recurrence and therapeutic resistance: phenotypic plasticity and adaptation to hypoxia. Longitudinal and single-cell studies have shown that GBM progression is driven less by new mutations and more by dynamic phenotype switching, most notably the adoption of a mesenchymal-like state [5]. This epithelial-to-mesenchymal transition (EMT)-like program enhances invasiveness and confers resistance to therapy. In parallel, hypoxia within the tumor core induces hypoxiainducible factor 1 (HIF-1α), which drives angiogenesis, metabolic reprogramming, invasion, and chemoresistance. HIF-1α upregulates Vascular Endothelial Growth Factor (VEGF) and synergizes with Epidermal Growth Factor Receptor (EGFR) and PI3K/ERK signaling, to amplify tumor progression [6, 7]. These hypoxia-driven angiogenic programs induce high vascularization in GBM and contribute to the resistance against anti-VEGF therapies such as bevacizumab or afatinib. Anyway, these therapies provide only modest clinical benefit [8]. Therefore, EMT and hypoxia-mediated signaling represent critical therapeutic challenges in GBM.

Within this framework, the formyl peptide receptor 2 (FPR2) emerges as a promising therapeutic candidate. FPR2 (also known as FPRL1 or ALX/FPR2) is a G protein–coupled receptor (GPCR) expressed in immune and neural cells, including neutrophils, monocytes, dendritic cells, astrocytes, and neurons [9, 10]. It responds to a broad range of ligands, from bacterial peptides to endogenous mediators such as lipoxin A4 (LXA4) and annexin A1. By regulating chemotaxis, cytokine release, and angiogenic signaling, FPR2 can modulate both inflammatory responses and tumor progression. Importantly, these functions may directly and profoundly interfere with GBM adaptive hallmarks: plasticity and hypoxia-driven angiogenesis. Dysregulated FPR2 activity has been implicated in several cancers [11–15], where it contributes to angiogenesis, tumor invasion, and metastasis [16, 17]. Evidence linking FPR2 to glioma development is continuously growing. Humanin, a mitochondrial peptide with cytoprotective properties, exerts protumorigenic effects in glioma cells through FPR2 [18]. Similarly, a tetrapeptide derived from *Androctonus australis* scorpion venom (AaTs-1) mimics the FPR2 agonist WKYMVm and promotes glioma proliferation via ERK, p38, and JNK phosphorylation [19]. Genomic profiling of IDH-wild-type GBM patients has additionally revealed potential pathogenic mutations in FPR2 [20]. Taken together, these findings suggest that FPR2 activation contributes to the GBM phenotype and represents a candidate target for therapeutic intervention.

Among endogenous ligands, LXA4 and its aspirin-triggered analog are notable for their potent antiinflammatory and pro-resolving actions [21]. They inhibit neutrophil recruitment, reduce cytokine production, and promote clearance of apoptotic cells, all limiting chronic inflammation and tumorpromoting microenvironment. In preclinical models of colorectal cancer, LXA4 suppresses tumor growth and angiogenesis [22, 23]. However, its clinical translation is limited by a poor

pharmacokinetic profile, including rapid inactivation by microglial cells via conversion to 15-oxo-LXA4 [24]. To address these limitations, synthetic FPR2 agonists have been developed. One of these compounds is MR-39, a novel selective FPR2 agonist with favorable pharmacokinetic properties and potent anti-inflammatory activity. MR-39 reduces pro-inflammatory mediators, such as interleukin-1β (IL-1β) and tumor necrosis factor-α. (TNF-α), in LPS-stimulated microglial cells [25]. Moreover, it demonstrates anti-inflammatory activity in LPS-stimulated organotypic hippocampal cultures [26] and shows blood–brain barrier permeability in hCMEC/D3 cells [25]. MR-39 also mitigates neuroinflammation in models of Alzheimer's disease [27] and autism spectrum disorders (ASD) [28]. Importantly, MR-39 showed no cytotoxicity in primary cultures of microglial cells or hippocampal neurons as well as in hippocampal organotypic under resting conditions [25, 26, 28] and did not induce genotoxicity in the Ames test (unpublished results). Additionally, chronic in vivo administration of MR-39 (10 mg/kg) for either twenty weeks or eight days did not induce any toxicity [27, 28], supporting the safety profile of this compound for use in living organisms.

Here, we investigate the effects of MR-39 on human GBM cell lines, focusing on processes having a key role in tumor progression: proliferation, motility, angiogenesis and hypoxia response. We also analyzed its impact on MAPK/ERK and AKT signaling pathways, cell cycle regulation, and EMT. By elucidating the role of FPR2 activation in GBM, this study aims to identify the mechanisms of action of MR-39 as a potential therapeutic candidate contributing to the development of innovative pharmacological strategies for this devastating disease.

Methods

Cell cultures

For this study we selected a panel of human GBM multiforme cell lines with different phenotypes: U87MG, an epithelial-like cell line derived from a malignant glioma in a male patient, known for rapid growth and high invasiveness; U138-MG, a polygonal adherent cell line derived from a grade IV glioblastoma in a male patient, characterized by slower growth and a stable karyotype; and U251-MG, an epithelial-like line from a female patient's malignant glioblastoma with moderate proliferative ability.

For angiogenesis assays, we used EA.hy926, a human immortalized endothelial cell line derived from the fusion of human umbilical vein endothelial cells (HUVECs) with the human lung carcinoma (A549) cell line.

All cells were cultured in plates in Dubecco's Modified Eagle Medium (DMEM) high glucose with sodium pyruvate with L-Glutamine (Euroclone, Milan, Italy # ECM0728L) supplemented with 10% fetal bovine serum (FBS, Euroclone #ECS5000L), 100 units/mL penicillin, and 100 µg/mL streptomycin (Euroclone #ECB3001D), and grown in a humidified 5% CO_2 at 37 °C, according to ATCC recommendations. The culture medium was replaced every three days to maintain optimal growth conditions.

EA.hy926 (CRL-2922 ™) andU87-MG (HTB-14 ™) cell lines were acquired from ATCC, while U138MG, and U251-MG were kindly provided by Prof. Generoso Luca Colucci D'Amato, University of Campania "Luigi Vanvitelli" [29].

Drugs and treatment

((S)-3-(4-Cyanophenyl)-N-[[1-(3-chloro-4-fluorophenyl)cyclopropyl]methyl]-2-[3-(4 fluorophenyl)ureido] propanamide)—compound MR-39 (CAS Registry Number 2169267-60-9) was synthesized in the laboratories of the University of Bari, as previously described [25].

MR-39 was dissolved in 100% DMSO to prepare a 10 mM stock solution (Sigma-Aldrich, Milan, Italy #2438), which was aliquoted and stored at − 20 °C to avoid repeated freeze–thaw cycles. For the in vitro experiment the stock solution was diluted in culture medium to obtain the desired working concentrations [28]. DMSO was used at concentrations below 0.1%, which is well within the range generally considered non-toxic and unlikely to interfere with the biological processes investigated in this study. To exclude any solvent-related effects, control cultures were treated with an equivalent final concentration of DMSO diluted in the culture medium.

WRW4 (Bio-Techne, Milan, Italy #2266/1), a selective antagonist of FPR2 signaling, was dissolved at 1 mg/ml in water, aliquoted, and stored at − 20 °C to prevent repeated freeze–thaw cycles. Glioblastoma cells were treated with MR-39 at concentrations ranging from 5 to 100 µM for 48 h, either alone or in combination with WRW4 (Bio-Techne) at concentrations of 5 to 100 µM.

Cell counting kit-8 assay

GBM cell lines (U87-MG, U138-MG, and U251-MG) were seeded at 1×10^4 cells/well in 96-well plates and grown for 24 h. The next day, the medium was replaced with fresh medium. Cells were treated with vehicle (CTRL, DMSO) or MR-39 and WRW4 (Bio-Techne), either alone or in combination, under the following conditions: (i) MR-39, 5-100 µM; (ii) WRW4 (Bio-Techne), 5-100 µM.

A concentration of ~ 10 µM MR-39 was identified as the lowest dose that significantly inhibited cell proliferation and was therefore selected for subsequent experiments, including (iii) 1 h pre-treatment with WRW4 (10 µM) followed by 48 h treatment with MR-39 (10 µM).

The antiproliferative activity was evaluated through the Cell Counting Kit-8 (CCK-8) assay (Enzo, Euroclone).

This method quantifies the reduction of WST-8 by live cells into a water-soluble yellow formazan, with the amount produced reflecting the number of viable cells. CCK-8 assay was performed by incubating cells with 10% CCK-8 solution for 1 h at 37 °C in 5% CO_2. Absorbance was measured at 450 nm using a microplate reader (Thermo Fisher Scientific, Milan, Italy).

Trypan blue assay

Total cells and percent viability were determined using the Trypan Blue exclusion assay (ThermoFisher Scientific). U87-MG, U138-MG, and U251-MG cell lines were seeded as described above and treated with vehicle (CTRL, DMSO) or 10 μM MR-39 for 48 h. Following treatment, the medium was removed, and the cells were harvested with trypsin-EDTA. A 10 μL aliquot of cell suspension was mixed 1:1 with 0.4% Trypan Blue solution. Total live cell count (cells/mL) and live/dead ratio were automatically determined using the TC20 automated cell counter (Bio-Rad, Milan, Italy).

Ki67 and HIF-1α Immunofluorescence staining

GBM cells (U87-MG and U138-MG) were seeded at a density of 1×10^4/well in a four-well μ-Slide (Ibidi) for Ki67 detection or at 2×10^4/well in a 24-well plate for HIF-1α analysis. For Ki67 staining, cells were incubated for 48 h with vehicle (CTRL, DMSO) or MR-39 (10 μM), whereas for HIF-1α detection, U87MG cells were treated with 100 μM cobalt chloride ($CoCl_2$, Carlo Erba; Milan, Italy, #439355) as a hypoxia inducer, alone or in combination with MR-39 (10 μM), for 48 h. After treatment, cells were fixed with 4% PFA (ThermoFisher Scientific), washed 3 times with PBS, permeabilized with either 0.3% Triton X-100 and blocked with 5% BSA in PBS (Ki67) or 0.1% Triton X-100 for 5 min followed by blocking with 3% BSA in PBS for 1 h (HIF-1α). For Ki67 staining, cells were incubated overnight at 4 °C with Ki67 (D3B5) antibody rabbit mAb Alexa Fluor 488 Conjugate (1:500, Cell Signaling, Milan, Italy #11882). For HIF-1α staining, cells were incubated overnight at 4 °C with anti-HIF-1α antibody (1:400, Cell Signaling #BK36169), followed by anti-rabbit IgG (H + L), F(ab')$_2$ Fragment (Alexa Fluor 488 Conjugate, Cell Signaling #4412). In both cases, nuclei were counterstained with DAPI (1:10000, Cell Signaling #4083), and fluorescence images were acquired using a confocal microscope (Zeiss LSM 900 Airyscan 2) with a 40× oil-immersion objective.

siRNA transfection

U87-MG cells were transfected with three different FPR2 antisense oligonucleotides (Silencer® Select siRNAs #4392420) purchased from ThermoFisher Scientific, and identified as siRNA1 (#S5354), siRNA2 (#S5355), siRNA3 (#S5356), or a negative control siRNA (#4390846). Briefly, U87-MG cells at 80% confluence were trypsinized and transfected in suspension in Opti-MEM I medium (Invitrogen, Carlsbad, CA), using siPORT NeoFX Transfection Agent (Invitrogen, Carlsbad, CA), according to the manufacturer's instructions. The three different siRNAs or the negative control were used at a final concentration of 30 nM. After 6 h, the transfection mix was replaced with complete medium. Then, the transfected and control cells were treated with MR-39 (10 μM) for an additional 48 h. At the end of the treatment, the CCK-8 assay was performed as previously described. To verify the effectiveness of the silencing, a qPCR analysis was performed as described below.

RNA-seq analysis

RNA extraction

Total RNA was extracted from biological replicates of control ($n = 3$) and MR-39-treated ($n = 2$) U87-MG pellets, snap frozen in dry ice immediately after harvest, with the NORGEN Total RNA extraction kit (#17200) according to the manufacturer's protocol. RNA concentration and quality were assessed using a Nanodrop spectrometer, Qubit Flex fluorimetry with the RNA High Sensitivity kit (Thermo Fisher Scientific #Q32852), and an Agilent Tapestation with High Sensitivity RNA ScreenTape (#5067–5579). RIN (RNA Integrity Number) obtained is reported in Table S1.

RNA-seq library preparation

To prepare the RNA-seq library for each biological replicate, we used the Illumina Stranded Total RNA prep. Ligation with Ribo-Zero Plus (#20040525) according to the manufacturer's protocol, starting with 500 ng RNA per sample (9.7 average RIN). After manual preparation, the concentration and quality of the libraries were assessed using an Agilent Tapestation and D2100 High Sensitivity DNA ScreenTape (#5067–5584), as well as a Qubit dsDNA BR Assay (ThermoFisher Scientific #Q32853), with satisfactory results. Molarity of the libraries was calculated to proceed with the sequencing.

Sequencing

10 μL of the obtained libraries (1 pM final loading concentration) were combined and used for sequencing with an Illumina High Output 150-cycle cartridge and flow cell (#20024907). 1% Phix library spike-in control was added to the final library pool, and the sequencing was performed on an Illumina NextSeq 550 sequencer. Those operative steps were performed according to the Illumina protocols.

Data analysis

Raw data were processed using the Illumina BaseSpace cloud workspace. Briefly, we obtained differential

expression data (DESeq2), heatmaps, and PCA charts using the Illumina DRAGEN RNA Pipeline (ver. 4.0.3) with standard parameters for alignment to GRCh38, proprietary mapping algorithm, and filtering with duplicate removal with standard parameters, as well. Pipeline generated the count files using the GENCODE annotation. Gene count data were imported into DESeq2 v1.36.o module in order to obtain the differential expression data after size factor normalization. Genes with p-adj < 0,05 (Benjamini–Hochberg) and | log2FoldChange| ≥ 1 were considered significantly modulated. Differential DESeq2 data were used to derive the list of down-regulated genes in treated vs. control U87-MG cells. Over-representation analysis (ORA) was performed on Gene Ontology—Biological Process (GO: BP) using the clusterProfiler R package with enrichGO.

RNA extraction and RT-qPCR analysis

RNA extraction was performed using the Total RNA Purification Kit (ThermoFisher Scientific #17200) according to the manufacturer's protocol. RNA concentration and quality were assessed by a Nanodrop spectrometer. Two micrograms of RNA were reverse transcribed using the LunaScript RT (New England Biolabs #E3010). Quantitative PCR was performed on 4 µl of previously diluted cDNA (1:4) template using Luna Universal qPCR Master Mix (New England Biolabs, #E3003), along with 0.25 µM of specific oligos (Eurofins Scientific, Milan, Italy) listed in Table S2. The Bio-Rad CFX96 Touch Real-Time PCR Detection System was used for the RT-qPCR run. Gene expression data were normalized to HMBS. The qPCR analysis was carried out on triplicate samples. The gene expression level of interest was then calculated as $2^{-\Delta\Delta CT}$, or $2^{-\Delta CT}$ where ΔCT = CT of the gene of interest - CT of HMBS.

Protein extraction and western blot analysis

Protein extraction was performed at 4 °C for 30 min using RIPA buffer (25 mM Tris–HCl, pH 7.4, 150 mM, NaCl, 5 mM EDTA, 5% (v/v) glycerol, 1% Triton) supplemented with 1X protease inhibitors (ThermoFisher Scientific) and phosphatase inhibitor (10 mM NaF, 1 mM Na_3OV_4, 1mM PMSF). The protein fraction was collected by centrifugation at 13,000 × g for 10 min at 4 °C. Protein concentration was determined using the Bradford assay (Bio-Rad Laboratories, Milan, Italy) according to the manufacturer's instructions.

For Western Blot analysis, protein samples (20 µg) from GBM cell lysates were separated by SDS-PAGE and transferred onto nitrocellulose or PVDF membranes. Membranes were then blocked at room temperature with 5% milk buffer (w/v). After 1 h, membranes were incubated overnight at 4 ∘C with the following primary antibodies: p-Akt (1:1000, Cell Signaling, #BK4060); Akt (1:1000, Cell Signaling #BK4691); β-actin (1:1000, Cell Signaling #BK3700); pERK (1:1000, Cell Signaling #BK4370); ERK (1:1000, Cell Signaling #BK9102); FN1 (1:500, ELK Biotechnology, Milan, Italy #ES2355); NF-kB p65 (1:1000, Cell Signaling #BK8242); p21 (1:1000, Cell Signaling #BK2947); p27 (1:1000, Cell Signaling #BK3698); p53 (1:1000, Cell Signaling #BK2524) and GAPDH (1:2500, Cell signaling #BK2118). Then, the membranes were incubated with the appropriate secondary antibodies (goat anti-rabbit IgG, Amersham, Milan, Italy, 1:5000, or anti-mouse IgG antibodies, Amersham, 1:5000) for 1 h. Chemiluminescence was detected using the ECL method (ECL, EuroClone #EMP012001) and visualized with a ChemiDOC imaging system (Bio-Rad). Densitometric analysis was performed using ImageJ software (version 1.54p) or Biorad Image Lab software.

FACS analysis

The cell cycle distribution of U87-MG cells treated with vehicle (CTRL, DMSO) or MR-39 (10 µM) alone or in combination with WRW4 (10 µM) was assessed using the Cell Cycle Assay Solution Deep Red Kit (Dojindo, Kumamoto, Japan) and performed according to the manufacturer's instructions. Samples were acquired using a BriCyte E6 flow cytometer (Mindray Medical Italy S.r.l., Milan, Italy), and data were analyzed using FlowJo software (TreeStar V.10; Carrboro, NC, USA).

Wound healing assay

U138-MG and U251-MG cells were seeded into 24-well plates at a density of 1.5×10^5 cells/well in serumfree medium. When cultures reached ~ 80% confluence, vertical scratches were made across the monolayer using a sterile pipette tip. Detached cells were removed by washing with PBS, and the remaining cells were treated with vehicle (CTRL, DMSO) or MR-39 (10 µM) alone or in combination with WRW4 (10 µM). Cell migration was monitored under a phase-contrast microscope (Leica DCF 3000G) at 10× magnification until wound closure.

In vitro tube formation assay

A 96-well plate was coated with 50 µL of Matrigel® Matrix (Growth Factor Reduced, Corning, Bedford, MA, USA) and incubated at 37 °C for 1 h. Subsequently, 1×10^4 EA.hy926 endothelial-like cells/well were seeded in serum-free medium and treated with or without MR-39 (10 µM). FBS was used as a positive control. Tube formation was monitored after 6 h using a phase-contrast microscope (Leica DCF 3000G) with a 10× magnification.

Statistical analysis

For each experimental condition, cultures were prepared in triplicate, and experiments were repeated using independent cell preparations. Data are expressed

as mean ± standard error of the mean (SEM). Statistical analyses were performed using GraphPad Prism 8.0 (GraphPad Software Inc., San Diego, CA, USA). Group differences were evaluated by one-way ANOVA followed by Tukey's post hoc test, or by unpaired Student's t-test, as appropriate. A p-value ≤ 0.05 was considered statistically significant.

Results

Antiproliferative effect of MR-39 on human glioblastoma cell lines

FPR2 has an emerging role in modulating inflammatory and proliferative signals in tumors [30]; however, its specific function in GBM remains largely uncharacterized. To address this aspect, we used MR-39, a novel synthetic compound that works as a selective FPR2 agonist (Figure S1A). To gain new insights into the role of FPR2 in GBM and its potential as a therapeutic target, we evaluated the effects of MR-39 on cell proliferation and viability.

To investigate the functional relevance of FPR2 activation in GBM, we selected three human GBM cell lines, U87-MG, U138-MG, and U251-MG, that exhibit distinct phenotypes but similar levels of FPR2 gene expression (Figure S1B). These cell lines were exposed to increasing concentrations of MR-39 (5-100 µM; Fig. 1A), and proliferation was assessed using the CCK-8 assay. As shown in Fig. 1A, MR-39 treatment significantly reduced proliferation in a dose-dependent manner across all three cell lines. Notably, a concentration of ~ 10 µM was identified as the lowest concentration with a significant antiproliferative effect, indicated by IC_{50} values of 12.56 µM (U87-MG), 12.82 µM (U138-MG), and 9.75 µM (U251-MG). This result was further confirmed by counting cells treated with 10 µM MR-39 and comparing this value with that of cells treated with vehicle only (Fig. 1B). Importantly, the observed reduction in proliferation was not accompanied by a decrease in cell viability, as determined by the trypan blue assay. This result suggests that

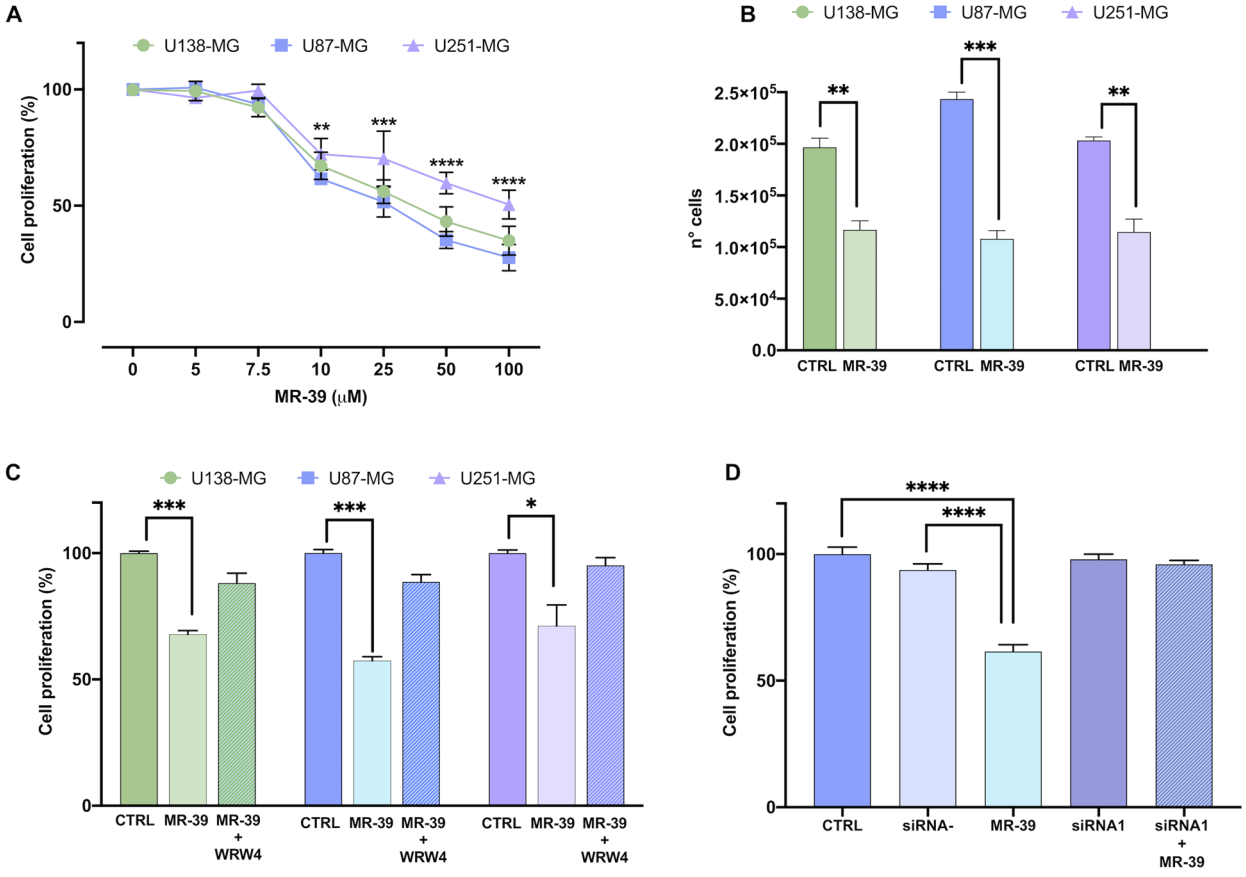

Fig. 1 Antiproliferative effect of MR-39 on human glioblastoma cell lines. (**A**) U87-MG, U138-MG, and U251-MG cells were exposed to 5-100 µM of MR-39 for 48 h. (**B**) Number of U87-MG, U138MG, and U251-MG cells exposed for 48 h to either the vehicle (CTRL) or 10 µM MR-39. (**C**) U87-MG, U138-MG, and U251-MG cells were exposed to either vehicle (CTRL) or 10 µM MR-39, with or without the FPR2 antagonist WRW4 (10 µM). (**D**) U87-MG cells were transfected with FPR2-targeting antisense siRNA1 or a negative control (siRNA-), followed by treatment with or without 10 µM MR-39. Cell proliferation was measured using the CCK-8 assay and is expressed as a percentage of the control. Data are expressed as means ± SEM, n = 3. Statistically significant differences are based on an unpaired t-test * p value < 0.05, ** p value < 0.005, *** p value < 0.001, **** p value < 0.0001 or one-way ANOVA followed by Tukey's multiple comparison test

MR-39 selectively slows proliferation rate and capacity without inducing cytotoxicity (Figure S1C).

To confirm the involvement of FPR2 in mediating the antiproliferative effect, GBM cells were pretreated with a selective FPR2 antagonist WRW4 for 1 h before MR-39 exposure. As shown in Fig. 1C, WRW4 significantly reversed the antiproliferative effects of MR-39, supporting the conclusion that FPR2 signaling is essential for this response. Notably, WRW4 alone, even at elevated concentrations, did not affect cell proliferation (Figure S1D), additionally supporting the specificity of MR-39 antiproliferative action. To further validate the role of FPR2, we silenced its expression in U87-MG cells using antisense oligonucleotides. We analyzed three siRNAs, but only siRNA1 showed efficient knockdown, reducing FPR2 expression by approximately 50%. In contrast, siRNA negative control, siRNA2, and siRNA3 showed no detectable effect on FPR2 expression (Figure S1E). When U87-MG cells were transfected with siRNA1 and subsequently treated with MR-39, the antiproliferative effect of the FPR2 agonist was markedly reduced, confirming that FPR2 activation is critical for mediating this response. In contrast, transfection with a negative control siRNA did not alter cell proliferation (Fig. 1D).

MR-39 suppresses glioblastoma cell proliferation via downregulation of Ki67 and inhibition of MAPK/ERK and AKT pathways

To identify the mechanisms by which MR-39 suppresses cell proliferation, we analyzed Ki67 expression, a well-known marker of cell proliferation [31]. Immunostaining showed a significant reduction in Ki67 levels in MR-39–treated U87-MG cells compared to control, demonstrating a substantial decrease in cell growth activity (Fig. 2A).

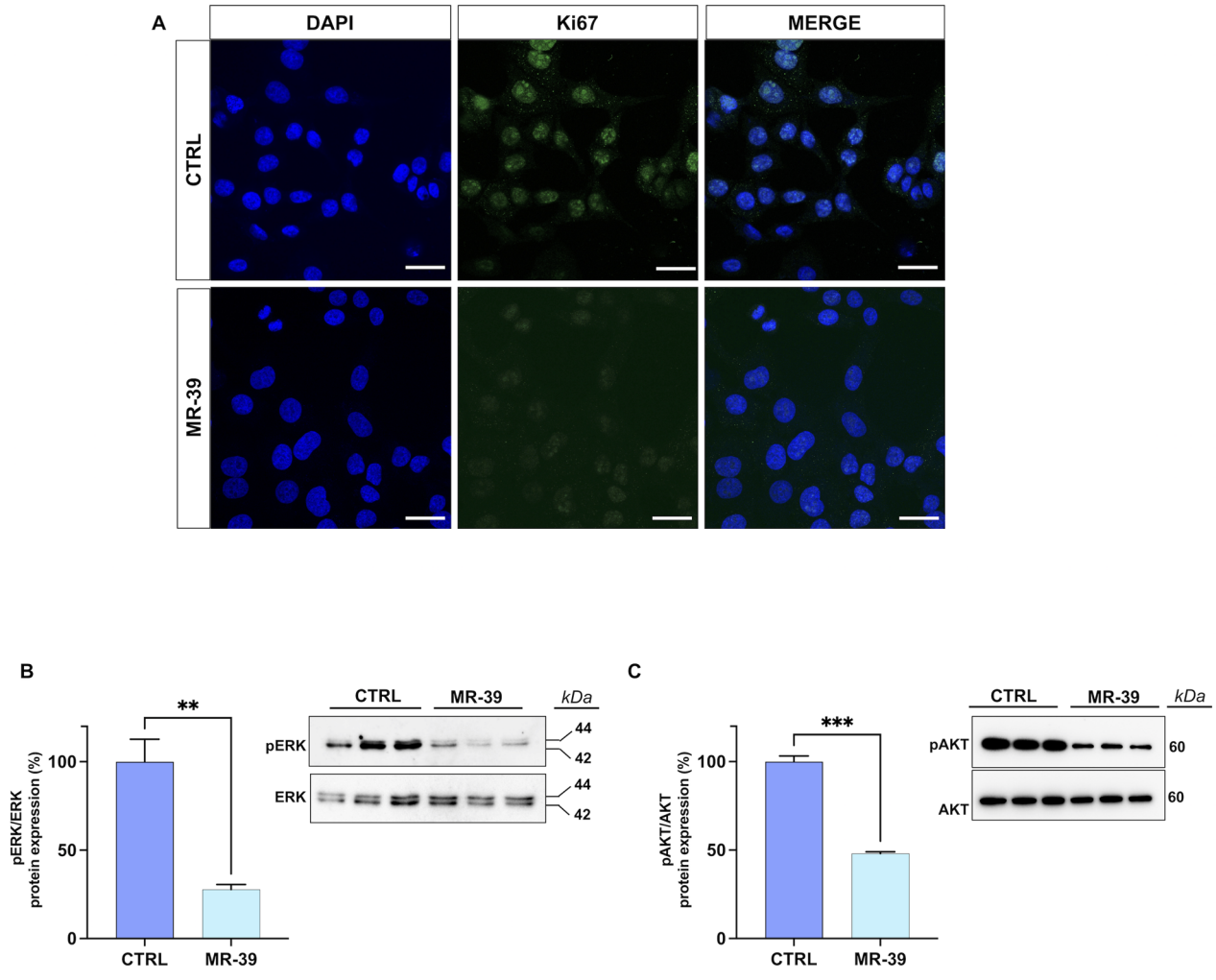

Fig. 2 Effect of MR-39 on cell proliferation and protein expression in U87-MG cells. (**A**) Representative images of U87-MG cells treated for 48 h with either vehicle (CTRL) or 10 µM MR-39, followed by staining with DAPI and Ki67 antibody, to assess proliferation. (**B**) pERK protein levels, normalized to total ERK, and (**C**) pAKT protein levels, normalized to total AKT, were measured in U87MG cells both vehicle-treated (CTRL) and treated with 10 µM MR-39 for 48 h Western blot images show the molecular weight of each protein (in kDa) on the right. Protein expression is presented as a percentage of the CTRL. Scale bar, 25 µm. Data are expressed as mean ± SEM (n = 3). Statistical significance was determined by an unpaired t-test (**p < 0.01, ***p < 0.001)

Thus, these data support the anti-proliferative effect of MR-39, as illustrated in Fig. 1. A similar reduction in Ki67 expression was also observed in U138-MG cells, suggesting that MR-39 antiproliferative effects are consistent across different glioblastoma models (Figure S2A).

In addition, MR-39 treatment led to an approximately 70% reduction in ERK1/2 phosphorylation (Fig. 2B). Given the crucial role of MAPK signaling in regulating cell cycle progression and proliferation [32], this inhibition is likely to contribute to the observed decrease in Ki67 expression.

Along with its impact on MAPK signaling, MR-39 also induced an about 50% decrease in AKT phosphorylation (pAKT, Fig. 2C). AKT is a key mediator of cell survival and proliferation (Fig. 2C) and its activation typically promotes cell cycle progression and metabolic regulation, while inhibiting apoptotic pathways [33]. The reduction in pAKT suggests that MR-39 suppressed pro-survival signaling, reinforcing its antiproliferative effects via multiple pathways.

MR-39 induces S-phase accumulation and disrupts cell cycle progression in glioblastoma cells

To further investigate how MR-39 affects cell cycle progression, we performed flow cytometric analysis on U87-MG cells treated with MR-39. The results showed an accumulation of cells in the S phase, paralleled by a significant reduction in the percentage of cells in the G2/M-phase population, suggesting that MR-39 disrupted normal cell cycle dynamics, possibly by delaying or arresting cells during DNA synthesis and preventing them from entering mitosis (Fig. 3A). These changes were also evident in U138-MG cells (Figure S2B).

To confirm that these effects were mediated through FPR2 signaling, U87-MG cells were pretreated with WRW4 before exposure to MR-39. As shown in Fig. 3A, WRW4 effectively reversed the MR-39–induced alterations in cell cycle distribution, restoring both the S and G2/M-phase populations to levels comparable to those of untreated controls.

In U87-MG cells, MR-39 treatment induced significant changes in the expression of genes involved in cell cycle arrest. In particular, MR-39 increased Cyclin D2 (CCND2) mRNA levels, a key regulator of the G1/S transition, and decreased Cyclin-Dependent Kinase 1 (CDK1) mRNA levels, which promote entry into mitosis (Fig. 3B). As a result, MR-39 prevented progression into mitosis, leading to cell accumulation in the S phase.

Interestingly, MR-39 also induced substantial changes in the expression of key cell-cycle regulatory proteins. As shown in Fig. 3C, treatment with MR-39 resulted in a significant upregulation of p53, a pivotal protein involved in the DNA damage response and cell cycle checkpoint regulation. In contrast, p27 levels were notably reduced (Fig. 3D), indicating that MR-39 promotes cell cycle progression, particularly from G1 to S, consistent with the observed increase in CCND2 levels, which further supported progression through the G1/S transition. The p21 expression remained unchanged (Fig. 3C), suggesting that MR-39 exerts a selective modulation of the p53 pathway in the absence of a full G1 arrest typically mediated by p21.

Whole transcriptome analysis of MR-39-treated glioblastoma cells

After confirming that the FPR2 agonist MR-39 inhibited proliferation in GBM cell lines, we investigated its effects on key tumor progression pathways, including migration, invasion, angiogenesis, and hypoxia response. In this context, we performed a whole-transcriptome analysis of GBM cells treated with MR-39. The expression profiles of biological replicates of U87-MG cells treated with MR-39 and controls were investigated to identify dysregulated genes involved in cell movement, invasion, angiogenesis, and hypoxia response. We first verified the Illumina DRAGEN RNA-seq pipeline's data and quality checks using a heatmap and principal component analysis (Figure S3A).

In particular, Principal Component Analysis (PCA) showed a clear separation between treated and control samples, confirming that the MR-39 treatment condition is the main source of transcriptional variability (Figure S3A). Similarly, the heatmap with the most variable genes showed a condition-related cluster with distinct expression pathways between treated and control groups (Figure S3B). Moreover, we performed pairwise comparisons between the two groups and explored the biological processes (BPs) enriched by the up- and down-regulated genes. GO BPs involved in cell movement, invasion, angiogenesis, and hypoxia response proliferation were identified as significantly downregulated in the MR-39-treated U87 compared to controls (-log10(p.adjust) > 3), as shown in the dot plot in Fig. 4A. To illustrate the complex gene architecture and the co-modulation between these pathways, we generated a CIRCOS plot for the Migratory (Fig. 4B), Angiogenesis (Fig. 4C), and Hypoxia (Fig. 4D) processes. Those graphs help the reader understanding of the main actors involved in modulating one or more of the mentioned GO BPs. The genes shown in the CIRCOS plots were all significantly modulated following the MR-39 treatment in U87-MG cells (-log10(p.adjust) > 3).

MR-39 interferes with epithelial-to-mesenchymal transition and angiogenic programs

Based on intriguing RNA-seq data and recognizing the critical role of EMT in promoting GBM invasiveness and resistance to therapy, we first examined whether

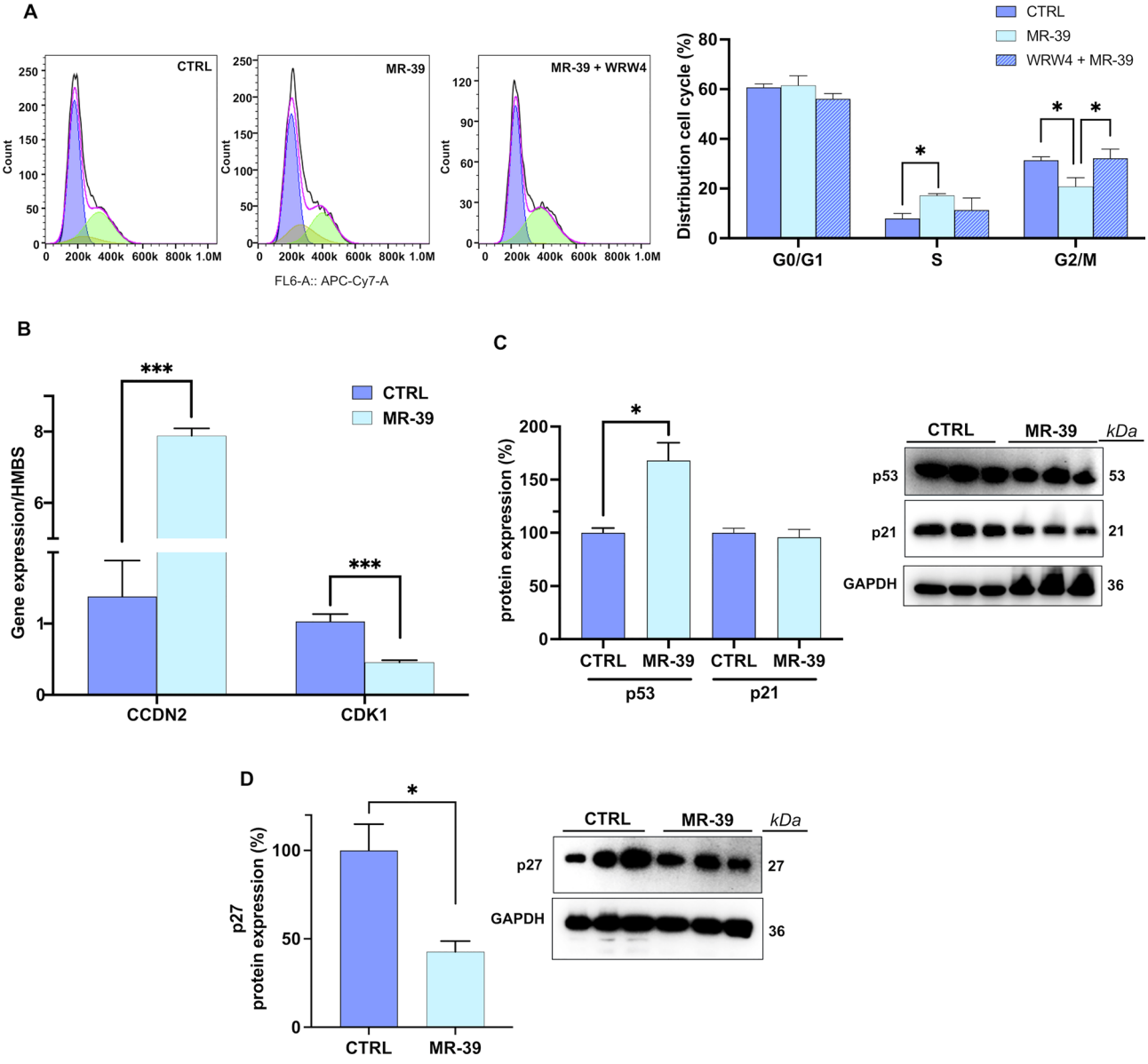

Fig. 3 Effects of MR-39 on cell cycle, mRNA, and protein expression in U87-MG cells. (**A**) Cell cycle distribution (in percentage) of U87-MG cells, both vehicle-treated (CTRL) or treated for 48 h with 10 μM MR-39, with or without the FPR2 antagonist WRW4 (10 μM). (**B**) CCND2 and CDK1 mRNA levels, normalized to HMBS, in U87-MG cells, both vehicle-treated (CTRL) or treated for 48 h with 10 μM MR-39. (**C**, **D**) p53, p21, and p27 protein levels, normalized to GAPDH, in vehicle-treated (CTRL) U87-MG cells or treated for 48 h with 10 μM MR-39. Western blot images show the molecular weight of each protein (in kDa) on the right. Protein expression is expressed as a percentage of the CTRL. Data are presented as mean ± SEM (n = 3). Statistical significance was determined by unpaired t-test (*p < 0.05, **p < 0.01, ***p < 0.001).

FPR2 activation by MR-39 affected genes involved in EMT and angiogenesis. We analyzed the expression levels of key EMT regulatory genes, including E-cadherin, N-cadherin, Slug, Snail, MMP-2, FN1, and Carboxypeptidase A4 (CPA4), in U87MG cells (Fig. 5A), through RT-qPCR. As shown in Fig. 5A, MR-39 increased E-cadherin expression levels, an epithelial marker that supports adherent junction stability. On the other hand, the treatment decreased N-cadherin, a mesenchymal marker associated with cell motility. These changes were consistent with the observed downregulation of Slug and Snail, which are transcriptional factors that repress Ecadherin (Fig. 5A). Interestingly, we also observed a significant reduction in genes involved in matrix remodeling, such as MMP-2, FN1, and CPA4 (Fig. 5A).

Moreover, to investigate MR-39's potential to interfere with angiogenesis, we analyzed the expression of two crucial mediators involved in angiogenic signaling and in maintaining vascular integrity in tumors: VEGF, which promotes endothelial cell proliferation, and

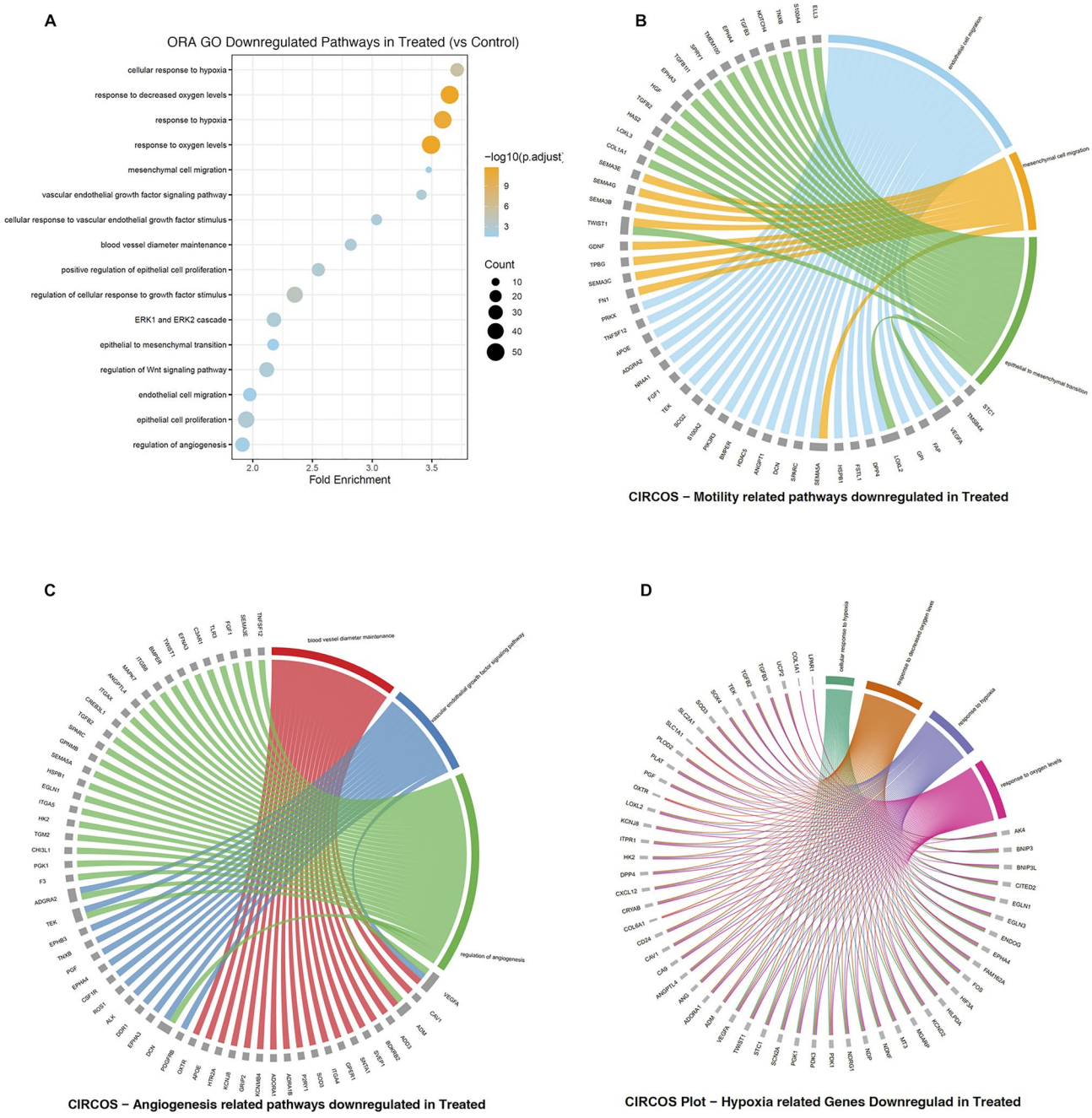

Fig. 4 Whole transcriptome analysis of MR-39-treated U87-MG cells. (**A**) GO BPs Dot Plot: The graph shows the downregulated Gene Ontology Biological Processes that are related to cell movement, invasion, angiogenesis, and hypoxia response. The Dots dimension indicates the number of mapped genes related to the pathway. On the X axis, the fold enrichment of the downregulated genes dataset is shown, and the color is related to the statistical significance (-log2 FC p.adjust). (**B**, **C**, **D**) Circos plot generated by mapping the downregulated genes in the MR39-treated U87 compared to controls. Migration/Invasionrelated processes (**B**); angiogenesis-related processes (**C**); hypoxia response-related processes (**D**)

VE-Cadherin, which is essential for stabilizing endothelial junctions during vessel proliferation. Consistent with RNA-seq data, exposure to MR-39 significantly reduced the expression of both genes (Fig. 5A). The U138-MG cell line showed a comparable trend in gene expression changes (Figure S4A). Transcriptional findings in U87-MG cells were supported by Western blot analysis, which confirmed that the reduction in mesenchymal state and the antiangiogenic effects of MR-39 treatment were paralleled by decreased protein levels of FN1 (Fig. 5B) and VEGF (Fig. 5C).

To functionally validate these molecular findings, we performed a wound-healing assay in U138-MG cells under serum-starvation conditions after MR-39

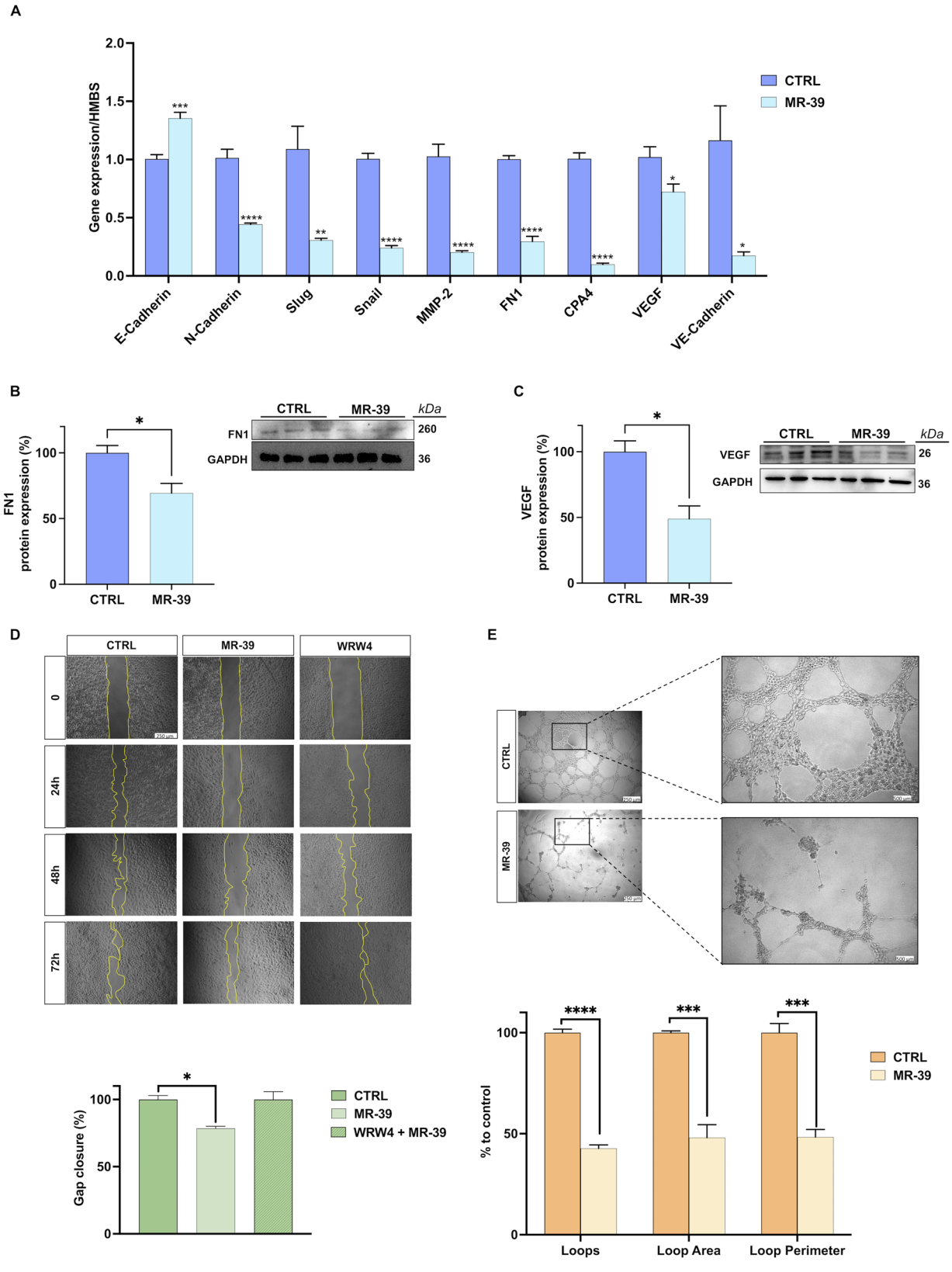

Fig. 5 (See legend on next page.)

(See figure on previous page.)

Fig. 5 MR-39 interferes with epithelial-to-mesenchymal transition and angiogenic programs. (**A**) mRNA levels of E-cadherin, N-cadherin, Slug, Snail, MMP-2, FN1, CPA4, VEGF, and VE-cadherin in U87-MG cells, both vehicle-treated (CTRL) or treated for 48 h with 10 µM MR-39, normalized to HMBS. (**B**, **C**) FN1 and VEGF protein levels in CTRL U87-MG or treated for 48 h with 10 µM MR39, normalized to GAPDH. Western blot images show the molecular weight of each protein (in *kDa*) on the right. Protein expression is presented as a percentage of the CTRL. (**D**) Representative images from the wound healing assay of U138-MG cells at 0, 24, 48, and 72 h following 48-hour treatment with vehicle (CTRL) or 10 µM MR-39, with or without the FPR2 antagonist WRW4 (10 µM). Scale bar: 250 µm. Percentage of gap closure in MR-39–treated U138-MG cells, with or without WRW4 (10 µM), normalized to CTRL. (**E**) Representative images of EA.hy926 endothelial cells treated for 48 h with vehicle (CTRL) or 10 µM MR-39, scale bar, 250 µm. The rectangle highlights the magnified area. Scale bar, 500 µm. Quantification of loops, loop area, and total loop formation in EA.hy926 cells, expressed as a percentage of the CTRL. Data are presented as mean ± SEM ($n = 3$). Statistical significance was determined by an unpaired t-test (*$p < 0.05$, **$p < 0.01$, ***$p < 0.001$, ****$p < 0.0001$) or one-way ANOVA followed by Tukey's multiple comparison test

treatment (Fig. 5D). MR-39 significantly inhibited gap closure by approximately 20%, an effect that was completely reversed by co-treatment with WRW4. Similar anti-migratory effects of MR-39 and their reversal by WRW4 were also observed in U251-MG cells (Figure S4A). These results demonstrated MR-39's ability to inhibit glioblastoma cell migration via FPR2 activation, highlighting its potential to impair both proliferation and motility across diverse GBM models.

Additionally, we performed an in vitro tube formation assay using EA.hy926 endothelial cells. As illustrated in Fig. 5E, MR-39 significantly suppressed endothelial network formation. Specifically, MR39 reduced loop formation, loop area, and loop perimeter by about 50%, highlighting its strong inhibitory effect on endothelial network formation. Overall, these findings emphasized the role of MR-39 in interfering with two key pathways involved in tumor progression: EMT and angiogenesis.

MR-39 inhibits the hypoxic response

Based on RNA-seq results, we examined MR-39's ability to influence hypoxic response pathways. Hypoxia plays a crucial role in the aggressiveness of GBM and the formation of new blood vessels [34]. To replicate this in vitro, U87-MG cells were treated with 100 µM $CoCl_2$ to simulate low-oxygen conditions. As shown in Fig. 6A 10 µM MR-39 treatment significantly decreased cell proliferation as previously reported, with an even greater reduction observed under hypoxic conditions. This suggested that MR-39 influenced hypoxia-related signaling, thereby potentiating its antiproliferative effects under low-oxygen conditions.

To investigate whether MR-39 modulates the hypoxic response, we assessed HIF-1α expression, a key transcription factor involved in hypoxia adaptation, via RT-qPCR (Fig. 6B) and immunofluorescence (Fig. 6C). As expected, $CoCl_2$ treatment strongly induced HIF-1α mRNA and protein expression (Fig. 6B, C). Remarkably, MR-39 treatment under hypoxia led to a marked decrease in HIF-1α expression, suggesting that MR-39 may counteract hypoxia-driven signaling by suppressing HIF-1α accumulation. In contrast, treatment of U87-MG cells with MR-39 alone, did not induce significant changes in HIF-1α expression (Fig. 6B, C), suggesting that MR-39 specifically modulates the hypoxic response rather than affecting HIF-1α stability under normal oxygen conditions.

MR-39 treatment suppresses the inflammatory response

As previously demonstrated, MR-39 exhibits anti-inflammatory properties in various neurological disorders [26, 28]. To further explore its potential in glioblastoma, we examined the expression of key inflammatory markers in U87-MG glioblastoma cells treated with 10 µM MR-39. Using RT-qPCR, we observed significant downregulation of mRNA levels for several pro-inflammatory genes, including COX2, CXCL-7, NFKB1, IL-1β, and IL-6, following MR-39 treatment (Fig. 7A). A similar trend in gene expression was observed in U138-MG cells, further supporting the consistency of MR-39's antiinflammatory effects across glioblastoma cell lines (Figure S5).

These results suggest that MR-39 effectively suppresses the expression of critical inflammatory mediators involved in glioblastoma pathogenesis. Consistently, Western blot analysis confirmed a significant reduction in NF-κB protein levels in U87-MG cells, indicating that MR-39 may inhibit the NF-κB signaling pathway, a central regulator of inflammation (Fig. 7B).

Overall, these findings provide compelling evidence that MR-39 exerts anti-inflammatory effects in glioblastoma, likely via modulation of the NF-κB signaling pathway. Future studies will further investigate this pathway to elucidate the molecular mechanisms underlying MR-39's anti-inflammatory activity in glioblastoma.

Discussion

This study reveals, for the first time, that selective activation of FPR2 by the synthetic agonist MR-39 drives strong anti-tumor effects in GBM models, shedding light on its underlying mechanism of action. Across three genetically distinct human GBM cell lines, MR-39 consistently inhibited proliferation, disrupted cell cycle progression, reduced migratory capacity, and suppressed gene programs related to angiogenesis and hypoxia response. These effects were validated through multiple independent assays, underscoring the strength of our findings.

The antiproliferative effect of MR-39 was confirmed by cell counts, CCK-8 assays, and reduced. Ki67 expression,

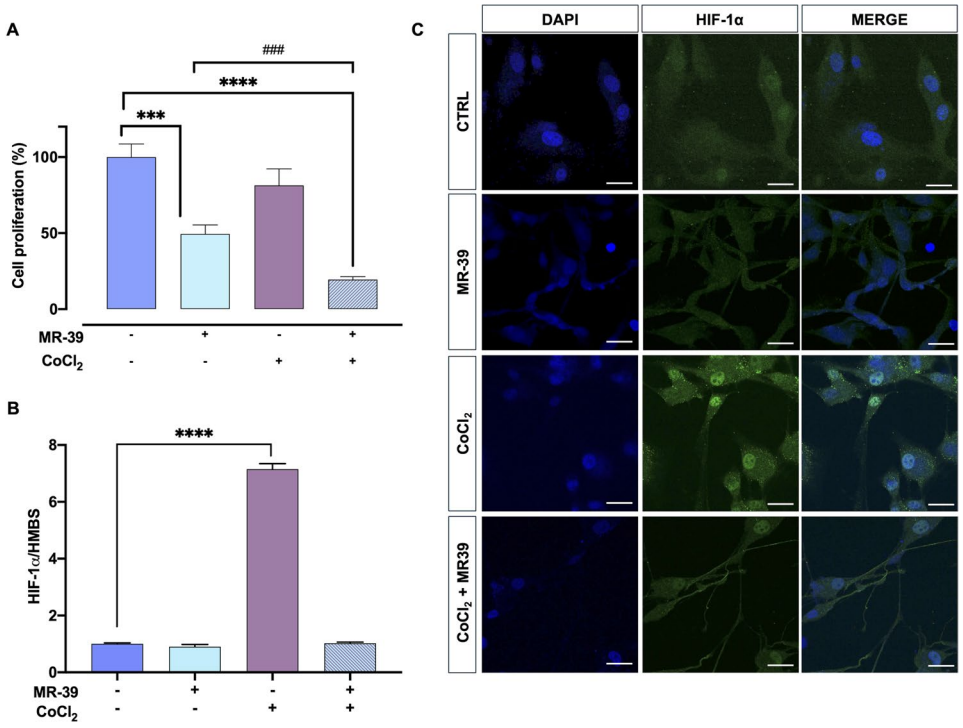

Fig. 6 MR-39 inhibits the hypoxic response in U87-MG cells. (**A**) U87-MG cells were treated with 100 µM cobalt chloride ($CoCl_2$) with or without 10 µM MR-39. Cell proliferation was assessed using the CCK-8 assay and is expressed as a percentage of the control. mRNA expression levels of HIF-1α in U87MG cells, treated with vehicle (CTRL), 100 µM cobalt chloride ($CoCl_2$), or 10 µM MR-39 (with or without $CoCl_2$), normalized to HMBS. (**C**) Representative images of U87-MG cells vehicle-treated (CTRL) or treated with 100 µM cobalt chloride ($CoCl_2$) with or without 10 µM MR-39, followed by staining with HIF1α antibody, DAPI, or both to assess hypoxia. Scale bar, 25 µm. Data are presented as mean ± SEM ($n = 3$). Statistical significance was determined by one-way ANOVA followed by Tukey's multiple comparison test (***$p < 0.001$, ****$p < 0.0001$, ###$p < 0.001$)

showing a predominantly cytostatic phenotype. Both pharmacological inhibition with the FPR2 antagonist WRW4 and genetic silencing of FPR2 abrogated MR-39 effects, confirming that MR-39 effects were specifically mediated by FPR2 activation. Mechanistically, MR-39 downregulated MAPK/ERK and AKT signaling, two oncogenic pathways frequently upregulated in GBM and strongly linked to poor prognosis [35]. This dual inhibition likely contributed to reduced proliferative capacity and altered cell cycle dynamics.

In canonical p53-mediated cell-cycle control, p53 activation induces p21, which inhibits CDK2 and leads to G1 arrest. In our study, however, MR-39 increased p53 levels while leaving p21 unchanged, thus cells accumulated in S phase rather than G1. This pattern indicates a non-canonical p53 response, in which p53 activation impacts S-phase progression independently of p21. Such atypical functions of p53 have been reported in GBM and other tumors, where p53 can regulate replication stress, DNA synthesis, and S-phase CDK activity through p21-independent mechanisms [36]. Consistently, MR-39 altered multiple S-phase regulatory proteins, including upregulation of Cyclin D2 and downregulation of CDK1 (a key driver of the G2/M transition), and reduction of p27 (a key inhibitor of CDKs involved in S-phase entry), creating an imbalance that slows or stalls S-phase transit without inducing apoptosis. While our findings support a model in which MR-39 engages a p53-dependent but p21-independent checkpoint, additional work will be necessary to define the precise molecular intermediates linking FPR2 activation to this non-canonical p53 response.

In addition to growth inhibition, MR-39 modulated the invasive phenotype of GBM cells. By upregulating E-cadherin and downregulating mesenchymal markers (N-cadherin, Slug, Snail) as well as extracellular matrix remodelers (MMP2, FN1, CPA4), MR-39 promoted a more epithelial-like state. Functional assays confirmed reduced wound-healing migration, an effect reversed by WRW4, additionally supporting FPR2-specific mediation. These findings indicate that MR-39 is a potential modulator of EMT, a central process that regulates GBM invasiveness and resistance to therapy.

Notably, recent single-cell multiomic studies have revealed that recurrent GBMs are characterized by a pronounced shift toward a mesenchymal phenotype, which is thought to underlie their plasticity and escape from targeted therapies [5]. This underscores the therapeutic relevance of our findings, as MR-39's ability to suppress mesenchymal programs and reinforce epithelial features

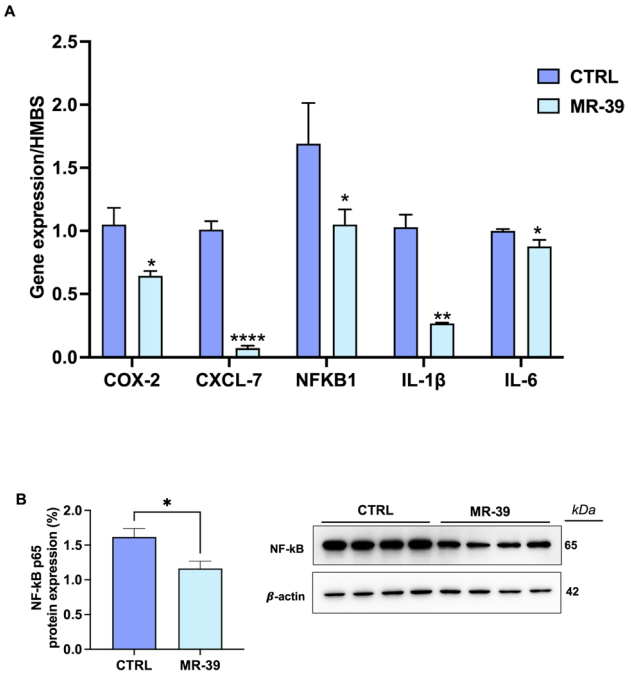

Fig. 7 MR-39 suppresses the inflammatory response in U87-MG cells. (**A**) mRNA levels of COX-2, CXCL7, NFKB1, IL-1β, and IL-6 in U87-MG cells, both vehicle-treated (CTRL) or treated for 48 h with 10 μM MR-39, normalized to HMBS. (**B**) NF-kB protein levels in CTRL U87-MG or treated for 48 h with 10 μM MR-39, normalized to β-actin. Western blot images show the molecular weight of each protein (in *kDa*) on the right. Protein expression is presented as a percentage of the CTRL. Statistical significance was determined by an unpaired t-test (*$p < 0.05$)

could directly counteract one of the key mechanisms driving GBM recurrence and treatment resistance.

MR-39 also interfered with angiogenic and hypoxic signaling, two hallmarks of GBM progression. Transcriptomic analysis, in addition to confirming impaired expression of EMT-related genes, revealed suppression of VEGF and VE-cadherin expression, which was confirmed at the protein level and functionally validated by impaired endothelial network formation in vitro. Significantly, MR-39 also attenuated HIF-1α accumulation under hypoxic conditions, thereby limiting one of the central adaptive mechanisms of GBM.

HIF-1α is a master regulator of GBM metabolism and progression, controlling glucose uptake, proliferation, migration, angiogenesis, and resistance through pathways such as EGFR, PI3K/AKT, and MAPK/ERK [6]. In addition, VEGF expression in GBM is regulated not only by hypoxia but also by EGF signaling, which converges on both MAPK/ERK and PI3K/RhoA/C pathways. Hypoxia, however, shifts VEGF regulation preferentially toward MAPK/ERK signaling while suppressing PI3K/RhoA/C activity [7]. Given that MR-39 suppresses VEGF, HIF-1α, and downstream MAPK/ERK and PI3K/AKT pathways, its activity appears to counteract multiple convergent mechanisms of hypoxia- and growth factor–driven angiogenesis. This suggests that MR-39 may block both angiogenic signaling and the adaptive plasticity by which GBM cells switch pathways in response to hypoxic stress. These results highlight the therapeutic relevance of MR-39, particularly given the limited clinical benefit of current anti-VEGF therapies, such as bevacizumab or afatinib. Despite its approval for recurrent GBM, bevacizumab primarily provides transient radiographic responses and symptomatic relief without significantly extending overall survival, reflecting the tumor capacity to activate alternative angiogenic and hypoxia-driven programs [8]. MR-39, by acting upstream of VEGF and simultaneously disrupting hypoxia-driven programs, may offer a complementary strategy to overcome the inherent resistance mechanisms of GBM. A limitation of this study is the use of $CoCl_2$, as a chemical model of hypoxia. While $CoCl_2$ stabilizes HIF-1α and reduces oxygen levels, it may also induce non-hypoxic effects, such as oxidative stress and cytotoxicity, which may not fully reflect the molecular responses occurring under true hypoxia. Consequently, the effects of MR-39 on hypoxia-related pathways should be further validated under controlled oxygen-deprivation conditions (e.g., hypoxia chambers or gas-controlled incubators) to confirm the physiological relevance of our findings.

MR-39, a patented compound originally developed for CNS disorders characterized by neuroinflammation [25], demonstrates significant therapeutic potential in GBM by modulating both hypoxic/angiogenic signaling and inflammatory pathways. In addition to its ability to inhibit angiogenesis, MR-39 exerts notable anti-inflammatory effects that may further enhance its efficacy in GBM treatment. While MR-39's anti-inflammatory properties have been well-documented in several CNS disease models [27, 28], our study provides the first evidence of its anti-inflammatory activity specifically in GBM. GBM is characterized by a highly inflammatory tumor microenvironment that supports tumor growth, fosters immune evasion, and contributes to resistance to therapy [37]. In this context, MR-39 treatment resulted in a marked downregulation of key pro-inflammatory genes, including COX-2, CXCL-7, NFKB1, IL-1β, and IL-6, which drive the inflammatory response in GBM. By suppressing these inflammatory mediators, MR39 may help alleviate the chronic inflammation that sustains tumor progression and immune suppression in GBM.

In addition to modulating these pro-inflammatory pathways, MR-39 also inhibited NF-κB activation, a critical regulator of inflammation and immune responses in GBM [38]. The suppression of NF-κB signaling suggests that MR-39 may reduce inflammation-driven tumor progression and enhance the effectiveness of immune-based therapies. Given the well-established role of inflammation in GBM aggressiveness and therapeutic resistance,

the dual action of MR-39 (targeting both inflammatory and oncogenic pathways), positions it as a promising therapeutic candidate for GBM treatment. Furthermore, MR-39 may overcome one of the significant challenges in GBM treatment: the blood-brain barrier. Indeed, recent findings demonstrate that MR-39 has favorable permeation properties in hCMEC/D3 cells, an established in vitro model of the BBB [25]. This suggests that MR-39 may efficiently cross the BBB, providing an important advantage for clinical application in treating GBM, where drug delivery is often hindered by the barrier's restrictive nature.

The therapeutic potential of MR-39 is further supported by its ability to engage FPR2 signaling in a ligand-specific and context-dependent manner. Whereas some FPR2 agonists, such as the scorpion venom-derived peptide AaTs-1 [19], promote glioma proliferation, MR-39 exerted the opposite effect, suppressing multiple oncogenic pathways. This divergence highlights the concept of biased agonism at FPR2: structurally diverse ligands can activate distinct downstream signaling pathways. By steering FPR2 signaling toward anti-tumor pathways, MR-39 showed the therapeutic potential of leveraging GPCR functional selectivity in cancer.

Taken together, these findings indicate that MR-39 targets key oncogenic and inflammatory pathways and may offers a potential strategy to overcome the challenges of GBM treatment, including immune evasion, resistance mechanisms, and BBB penetration. Future studies will deeper investigate the molecular mechanisms by which MR-39 modulates inflammation and exerts anti-tumor properties, potentially offering a more comprehensive and therapeutic approach for this highly aggressive malignancy.

Conclusions

Overall, our findings identify MR-39 as a promising therapeutic candidate for GBM. By selectively modulating FPR2 signaling, MR-39 inhibited proliferation, EMT-driven invasion, angiogenesis, hypoxic adaptation, and inflammation while enforcing a unique non-canonical S-phase arrest. These effects suggest that MR-39 can reprogram FPR2 signaling in glioblastoma cells toward a tumor-suppressive pathway. Collectively, our results highlight the therapeutic potential of FPR2 as a drug target and underscore the role of ligand-specific signaling in dictating GPCR functional outcomes. If validated in preclinical models, MR39 represents a valuable addition to the currently limited treatment options for GBM.

Abbreviations

AKT	AKT Serine/Threonine Kinase 1
ASD	Autism Spectrum Disorder
CCK-8	Cell Counting Kit-8
CCND2	Cyclin D2
CDK1	Cyclin-Dependent Kinase 1
COX-2	Cyclooxygenase 2
CPA4	Carboxypeptidase A4
CXCL7	Chemokine (C-X-C Motif) Ligand 7
E-cadherin	Epithelial Cadherin
EGRF	Epidermal Growth Factor Receptor
EMT	Epithelial-to-Mesenchymal Transition
ERK	Extracellular Signal-Regulated Kinase
FN1	Fibronectin 1
FPR2	Formyl Peptide Receptor 2
GBM	Glioblastoma
GO:BP	Gene Ontology:Biological Process
GPCR	G-Coupled Receptor
HIF-1α	Hypoxia Inducible Factor Subunit 1 Alpha
IL-1β	Interleukin-1β
IL-6	Interleukin-6
LXA4	Lipoxin A4
MAPK	Mitogen-Activated Protein Kinase
MMP2	Matrix Metallopeptidase 2
N-cadherin	Neural Cadherin
NFKB1	Nuclear Factor Kappa B Subunit 1
ORA	Over-Representation Analysis
PCA	Principal Component Analysis
RIN	RNA Integrity Number
RNA-seq	RNA sequencing
siRNA	Small Interfering RNA
SLUG	Snail Family Transcriptional Repressor 2
SNAIL	Snail Family Transcriptional Repressor 1

Supplementary Information

The online version contains supplementary material available at https://doi.org/10.1186/s12967-026-07781-3.

Supplementary Material 1

Supplementary Material 2

Supplementary Material 3

Supplementary Material 4

Supplementary Material 5

Supplementary Material 6

Supplementary Material 7

Supplementary Material 8

Supplementary Material 9

Acknowledgements

We thank Prof. Generoso Luca Colucci D'Amato, University of Campania "Luigi Vanvitelli" for generously providing the U138-MG and U251-MG glioblastoma cell lines used in this study.

Author contributions

Conceptualization: FV, MGF; Methodology: MGF, MB, MA, KDF, GE, LS; ML, EL; Formal analysis and investigation: MGF, MB, KDF, GE; Writing - original draft preparation: FV, MGF, MB; Writing - review and editing: FV, MGF, MB, GE, MC, LS, MC, AC, CPC, MCM, EL, ML; Funding acquisition: CPC, MCM; Supervision: FV.

Funding

This work was supported by NEXTGENERATIONEU (NGEU) and funded by the Ministry of University and Research (MUR), National Recovery and Resilience Plan (NRRP), project MNESYS (PE0000006) – A Multiscale integrated approach to the study of the nervous system in health and disease (DN. 1553. 11.10.2022). Partially by PRIN 2022 PNRR, European Union-Next Generation EU (project n. P20225W97A - Targeting the serotonin receptor 7 as a therapeutic approach for Angelman Syndrome).

Data availability
The raw data supporting the findings of this study are available from the corresponding authors upon reasonable request.

Declarations

Ethical approval
Not applicable.

Consent for publication
All authors have reviewed and approved the manuscript for submission to the Journal of Translational Medicine.

Competing interests
The authors declare no potential conflicts of interest related to this work.

Author details
[1]Department of Molecular Medicine and Medical Biotechnology, School of Medicine and Surgery, University of Naples Federico II, 80131 Naples, Italy
[2]Department of Life Sciences, Health and Health Professions, Link Campus University, 00165 Rome, Italy
[3]Department of Precision Medicine, University of Campania "Luigi Vanvitelli", 80131 Naples, Italy
[4]Molecular Oncology and Precision Medicine Laboratory, Biogem IRGS, 83031 Ariano Irpino, Italy
[5]Department of Pharmacy, School of Medicine and Surgery, University of Naples Federico II, 80131 Naples, Italy
[6]Department of Pharmacy-Drug Sciences, University of Bari Aldo Moro, 70125 Bari, Italy
[7]Department of Biology, University of Naples Federico II, 80126 Naples, Italy
[8]Medical Oncology, Fondazione Policlinico Universitario Agostino Gemelli IRCCS-Università Cattolica del Sacro Cuore, Rome, Italy
[9]Present address: CEINGE-Biotecnologie Avanzate s.c.ar.l., 80145 Naples, Italy

Received: 13 October 2025 / Accepted: 23 January 2026
Published online: 06 February 2026

References

1. Schaff LR, Mellinghoff IK. Glioblastoma and other primary brain malignancies in adults: A review. JAMA. 2023;329:574. https://doi.org/10.1001/jama.2023.0023.
2. Colopi A, Fuda S, Santi S, Onorato A, Cesarini V, Salvati M, et al. Impact of age and gender on glioblastoma onset, progression, and management. Mech Ageing Dev. 2023;211:111801. https://doi.org/10.1016/j.mad.2023.111801.
3. Vigneswaran K, Neill S, Hadjipanayis CG. Beyond the world health organization grading of infiltrating gliomas: advances in the molecular genetics of glioma classification. Ann Transl Med. 2015;3:95. https://doi.org/10.3978/j.issn.2305-5839.2015.03.57.
4. Stupp R, Van Den Mason WP, Weller M, Fisher B, Taphoorn MJB, et al. Radiotherapy plus concomitant and adjuvant Temozolomide for glioblastoma. N Engl J Med. 2005;352:987–96. https://doi.org/10.1056/NEJMoa043330.
5. Wang L, Jung J, Babikir H, Shamardani K, Jain S, Feng X, et al. A single-cell atlas of glioblastoma evolution under therapy reveals cell-intrinsic and cell-extrinsic therapeutic targets. Nat Cancer. 2022;3:1534–52. https://doi.org/10.1038/s43018-022-00475-x.
6. Wang G, Wang J-J, Fu X-L, Guang R, To S-ST. Advances in the targeting of HIF-1α and future therapeutic strategies for glioblastoma multiforme. Oncol Rep. 2017;37:657–70. https://doi.org/10.3892/or.2016.5309.
7. Nicolas S, Abdellatef S, Haddad MA, Fakhoury I, El-Sibai M, Hypoxia EGF, Stimulation Regulate. VEGF expression in human glioblastoma multiforme (GBM) cells by differential regulation of the PI3K/Rho-GTPase and MAPK pathways. Cells. 2019;8:1397. https://doi.org/10.3390/cells8111397.
8. Liu X. Treatment mechanism and research progress of bevacizumab for glioblastoma. Am J Cancer Res. 2025;15:1874–901. https://doi.org/10.62347/RNUE7193.
9. Serhan CN. Resolution phase of inflammation: novel endogenous Anti-Inflammatory and proresolving lipid mediators and pathways. Annu Rev Immunol. 2007;25:101–37. https://doi.org/10.1146/annurev.immunol.25.022106.141647.
10. Becker EL, Forouhar FA, Grunnet ML, Boulay F, Tardif M, Bormann B-J, et al. Broad immunocytochemical localization of the formylpeptide receptor in human organs, tissues, and cells. Cell Tissue Res. 1998;292:129–35. https://doi.org/10.1007/s004410051042.
11. Le Y, Oppenheim J, Wang J. Pleiotropic roles of formyl peptide receptors. Cytokine Growth Factor Rev. 2001;12:91–105. https://doi.org/10.1016/S1359-6101(01)00003-X.
12. Migeotte I, Communi D, Parmentier M. Formyl peptide receptors: A promiscuous subfamily of G protein-coupled receptors controlling immune responses. Cytokine Growth Factor Rev. 2006;17:501–19. https://doi.org/10.1016/j.cytogfr.2006.09.009.
13. Bae Y-S, Song JY, Kim Y, He R, Ye RD, Kwak J-Y, et al. Differential activation of formyl peptide receptor signaling by peptide ligands. Mol Pharmacol. 2003;64:841–7. https://doi.org/10.1124/mol.64.4.841.
14. Trojan E, Bryniarska N, Leśkiewicz M, Regulska M, Chamera K, Szuster-Głuszczak M, et al. The contribution of formyl peptide receptor dysfunction to the course of neuroinflammation: A potential role in the brain pathology. CN. 2020;18:229–49. https://doi.org/10.2174/1570159X17666191019170244.
15. Mastromarino M, Lacivita E, Colabufo NA, Leopoldo M. G-Protein coupled receptors involved in the resolution of inflammation: ligands and therapeutic perspectives. MRMC. 2021;20:2090–103. https://doi.org/10.2174/1389557520666200719014433.
16. Hou X-L, Ji C-D, Tang J, Wang Y-X, Xiang D-F, Li H-Q, et al. FPR2 promotes invasion and metastasis of gastric cancer cells and predicts the prognosis of patients. Sci Rep. 2017;7:3153. https://doi.org/10.1038/s41598-017-03368-7.
17. Lu J, Zhao J, Jia C, Zhou L, Cai Y, Ni J, et al. FPR2 enhances colorectal cancer progression by promoting EMT process. Neo. 2019;66:785–91. https://doi.org/10.4149/Neo_2018_181123N890.
18. Peña Agudelo JA, Pidre ML, Garcia Fallit M, Pérez Küper M, Zuccato C, Nicola Candia AJ, et al. Mitochondrial peptide humanin facilitates chemoresistance in glioblastoma cells. Cancers (Basel). 2023;15:4061. https://doi.org/10.3390/cancers15164061.
19. Aissaoui-Zid D, Saada M-C, Moslah W, Potier-Cartereau M, Lemettre A, Othman H, et al. AaTs-1: A tetrapeptide from androctonus australis Scorpion Venom, inhibiting U87 glioblastoma cells proliferation by p53 and FPRL-1 Up-Regulations. Molecules. 2021;26:7610. https://doi.org/10.3390/molecules26247610.
20. Chanez B, Appay R, Guille A, Lagarde A, Colin C, Adelaide J, et al. Genomic analysis of paired IDHwt glioblastomas reveals recurrent alterations of MPDZ at relapse after radiotherapy and chemotherapy. J Neurol Sci. 2022;436:120207. https://doi.org/10.1016/j.jns.2022.120207.
21. Suchitha GP, Devasahayam Arokia Balaya R, Prasad TSK, Dagamajalu S. A signaling network map of Lipoxin (LXA4): an anti-inflammatory molecule. Inflamm Res. 2024;73:1099–106. https://doi.org/10.1007/s00011-024-01885-6.
22. Liu H, Zeng J, Huang W, Xu Q, Ye D, Sun R, et al. Colorectal cancer is associated with a deficiency of Lipoxin A_4, an endogenous Anti-inflammatory mediator. J Cancer. 2019;10:4719–30. https://doi.org/10.7150/jca.32456.
23. Zong L, Chen K, Jiang Z, Chen X, Sun L, Ma J, et al. Lipoxin A4 reverses mesenchymal phenotypes to attenuate invasion and metastasis via the Inhibition of autocrine TGF-β1 signaling in pancreatic cancer. J Exp Clin Cancer Res. 2017;36:181. https://doi.org/10.1186/s13046-017-0655-5.
24. Romano M, Lipoxin, Aspirin-Triggered Lipoxins. Sci World J. 2010;10:1048–64. https://doi.org/10.1100/tsw.2010.113.
25. Stama ML, Ślusarczyk J, Lacivita E, Kirpotina LN, Schepetkin IA, Chamera K, et al. Novel Ureidopropanamide based N-formyl peptide receptor 2 (FPR2) agonists with potential application for central nervous system disorders characterized by neuroinflammation. Eur J Med Chem. 2017;141:703–20. https://doi.org/10.1016/j.ejmech.2017.09.023.
26. Trojan E, Tylek K, Leśkiewicz M, Lasoń W, Brandenburg L-O, Leopoldo M, et al. The N-Formyl peptide receptor 2 (FPR2) agonist MR-39 exhibits Anti-Inflammatory activity in LPS-Stimulated organotypic hippocampal cultures. Cells. 2021;10:1524. https://doi.org/10.3390/cells10061524.
27. Trojan E, Tylek K, Schröder N, Kahl I, Brandenburg L-O, Mastromarino M, et al. The N-Formyl peptide receptor 2 (FPR2) agonist MR-39 improves ex vivo and in vivo amyloid beta (1–42)-Induced neuroinflammation in mouse models of alzheimer's disease. Mol Neurobiol. 2021;58:6203–21. https://doi.org/10.1007/s12035-021-02543-2.

28. Cristiano C, Volpicelli F, Crispino M, Lacivita E, Russo R, Leopoldo M, et al. Behavioral, AntiInflammatory, and neuroprotective effects of a novel FPR2 agonist in two mouse models of autism. Pharmaceuticals. 2022;15:161. https://doi.org/10.3390/ph15020161.
29. Gentile MT, Ciniglia C, Reccia MG, Volpicelli F, Gatti M, Thellung S, et al. G Condorelli editor 2015 Ruta graveolens L. Induces death of glioblastoma cells and neural Progenitors, but not of Neurons, via ERK 1/2 and AKT activation. PLoS ONE 10 e0118864 https://doi.org/10.1371/journal.pone.0118864.
30. Zhao H, Wu L, Yan G, Chen Y, Zhou M, Wu Y, et al. Inflammation and tumor progression: signaling pathways and targeted intervention. Sig Transduct Target Ther. 2021;6:263. https://doi.org/10.1038/s41392-021-00658-5.
31. Scholzen T, Gerdes J. The Ki-67 protein: from the known and the unknown. J Cell Phys. 2000;182:311–22. https://doi.org/10.1002/(SICI)1097-4652(200003)182:3%253C311::AID-JCP1%253E3.0.CO;2-9.
32. Probstmeier R. Pharmacological targeting of the constitutively activated MEK/MAPK-dependent signaling pathway in glioma cells inhibits cell proliferation and migration. Int J Oncol [Internet]. 2011. https://doi.org/10.3892/ijo.2011.1165. [cited 2025 Aug 26].
33. McCubrey JA, Steelman LS, Abrams SL, Lee JT, Chang F, Bertrand FE, et al. Roles of the RAF/MEK/ERK and PI3K/PTEN/AKT pathways in malignant transformation and drug resistance. Adv Enzyme Regul. 2006;46:249–79. https://doi.org/10.1016/j.advenzreg.2006.01.004.
34. Kalkan R. Hypoxia is the driving force behind GBM and could be a new tool in GBM treatment. Crit Rev Eukaryot Gene Expr. 2015;25:363–9. https://doi.org/10.1615/CritRevEukaryotGeneExpr.2015015601.
35. Hasan S, Mahmud Z, Hossain M, Islam S. Harnessing the role of aberrant cell signaling pathways in glioblastoma multiforme: a prospect towards the targeted therapy. Mol Biol Rep. 2024;51:1069. https://doi.org/10.1007/s11033-024-09996-3.
36. Wagenknecht B, Hermisson M, Eitel K, Weller M. Proteasome inhibitors induce p53/p21Independent apoptosis in human glioma cells. Cell Physiol Biochem. 1999;9:117–25. https://doi.org/10.1159/000016308.
37. Nóbrega AHL, Pimentel RS, Prado AP, Garcia J, Frozza RL, Bernardi A. Neuroinflammation in glioblastoma: the role of the microenvironmentin tumour progression. CCDT. 2024;24:579–94. https://doi.org/10.2174/0115680096265849231031101449.
38. Ramar V, Guo S, Wang G, Liu M. The pivotal role of NF-κB in glioblastoma: mechanisms of activation and therapeutic implications. IJMS. 2025;26:7883. https://doi.org/10.3390/ijms26167883.

Publisher's note